Materials Research Bulletin 74 (2016) 27–33

Contents lists available at ScienceDirect

Materials Research Bulletin

journal homepage: www.elsevier.com/locate/matresbu

Crystal and electronic characterization of $Nd_xTi_{1-x}BO_{2+d}$ semiconductors

Osman Murat Ozkendir*

Mersin University, Faculty of Technology, Energy Systems Engineering, Tarsus, Turkey

ARTICLE INFO

Article history:
Received 30 April 2015
Received in revised form 14 September 2015
Accepted 6 October 2015
Available online xxx

PACS:
71.20.Be
71.20.Eh
71.20.Nr
74.25.Jb

Keywords:
Oxides
Semiconductors
XAFS (EXAFS and XANES)
Electronic structure
Crystal structure

ABSTRACT

Neodymium substituted $TiBO_3$ samples were investigated according to their crystal, electric and electronic properties. Studies were conducted by X-ray absorption fine structure spectroscopy (XAFS) technique for the samples with different substitutions in the preparation processes. To achieve better crystal structure results during the study, XRD pattern results were supported by extended-XAFS (EXAFS) analysis. The electronic structure analysis were studied by X-ray absorption near-edge structure spectroscopy (XANES) measurements at the room temperatures. Due to the substituted Nd atoms, prominent changes in crystal structure, new crystal geometries for Nd-Ti complexes, phase transitions in the crystals structure were detected according to the increasing Nd substitutions in the samples. In the entire stages of the substitutions, Nd atoms were observed as governing the whole phenomena due to their dominant characteristics in Ti geometries. Besides, electrical resistivity decay was determined in the materials with the increasing amount of Nd substitution.

1. Introduction

With the high potential in technological applications and vast preferable electrical, electronic and magnetic properties, Rare-Earth orthoborates find places in the center of materials' studies. Especially, the interactions occurring between 3d transition metals (TM) and 4f rare-earths (RE), attracts huge attentions of scientists' and cause a high demand to study on these materials. Narrow band structure and rich quantum symmetries of RE 4f levels are also known as governing the molecular interactions between their neighboring atoms. On the other hand, 3d levels of the transition metals build up links between the neighboring heavier and light atoms by bonding strongly to the heavy RE's 4f electrons with 2p electrons of the light atoms (i.e. O, S, B etc.) with a f–d–p hybridization. The presence of 3d levels of the TM's provide rich quantum symmetries for their neighbors and support the molecular reactions against the dipole selection rules. Besides, transition metals and their oxides are also leading materials in significant areas for future technologies because of having wished chemical, crystallographic, magnetic and electronic transport properties [1–3]. Their partly filled d shells emerge strong electronic correlations with the outer shell electrons of the neighboring atoms and play an important role causing a large variety of interesting physical phenomena.

In this study, the influence of Nd substitutions on the electronic and crystal structure properties of the $TiBO_3$ samples were investigated. $(Nd_xTi_{1-x})BO_{2+d}$ was considered as the general formula of the compounds where Boron is a key agent. The Borates are popular topics for the recent researches on materials where boron plays an important role because of its higher affinity, electron shortage and the vacant p-orbital. High thermal stability in the compounds and the luminescence properties make borates an important tool for high temperature and nonlinear optical materials [4].

$TiBO_3$ is the main part of the study and it is a member of MBO_3 group. Unfortunately, there is not so much study found in the literature on this material yet. Xu et al. were reported $TiBO_3$ as an insulator showing weak antiferromagnetic (AFM) ordering at around $T_N = 25$ under zero field cooled (ZFC) studies. However, under 500 Oe magnetic field, field cooled (FC) magnetic susceptibility studies showed weak ferromagnetic (FM) ordering. Besides, in the same study, $TiBO_3$ had also been reported as showing a diamagnetic behavior, which suppressed at a critical field of 500 Oe in the zero-field-cooling (ZFC) magnetic susceptibility

* Corresponding author. Fax: +903246274805.
E-mail address: ozkendir@gmail.com (O.M. Ozkendir).

http://dx.doi.org/10.1016/j.materresbull.2015.10.013
0025-5408/

measurements [5]. For the current $(Nd_xTi_{1-x})BO_{2+d}$ study, the samples were tested under 1 kOe FC magnetic susceptibility in a temperature range 300-5 K to probe the magnetic behaviors, however no specific magnetic behavior detected.

2. Materials and method

$Nd_xTi_{1-x}BO_{2+d}$ samples, where x has value as 0, 0.2, 0.4, 0.6, 0.8 and 1, were prepared by the solid-state reaction method at the MEITAM laboratories of Mersin University (Mersin, Turkey). The samples synthesized from the stoichiometric mixtures of Nd_2O_3, TiO_2 and B_2O_3 powder compounds as starting materials with high purity (>99.99%). The solid-state reaction method is the most used method for the preparation of bulk and powder materials by mixing parent materials. In such a method, mixing the powders does not start the reaction at room temperature. To obtain the best results for a desired material, the mixed materials should be milled and annealed to higher temperatures, like 700-1500 °C until the desired reactions take place. In this study, due to the higher electronegativity of Boron, the parent oxide B_2O_3 tend to isolate itself from reaction among other mixed oxides until 500 °C (given melting points of B_2O_3 in literature are: 450 °C (trigonal) and 510 °C (tetrahedral)). Beyond this temperature, the B_2O_3 oxides either react with other oxide groups to form the crystals or melt away from the material. So, to achieve better crystal formations in the samples, it was decided to anneal the samples in two steps; first up to 550 °C (close to the melting point of B_2O_3) and 950 °C (much above the melting point of B_2O_3). In the first step, the mixed powders milled for 30 min and annealed in air at 550 °C for 4 h. After the first annealing, as the second step, the mixed powders milled again for 30 min and samples annealed in air at 950 °C for 48 h.

To obtain the informations for the mechanisms of the crystal structure formations in the samples, the X-ray absorption fine structure spectroscopy (XAFS) measurements were performed. XAFS data can yield fruitful information to support the data derived from the XRD and performed resistivity measurements of the samples with four probe technique. This technique is one the best tool for providing a rich data collection for detailed electronic and crystal structure analysis of the materials. The XAFS data can be divided into two sections for analysis as XANES (X-ray absorption near-edge spectroscopy) and EXAFS (extended-XAFS).

The XANES region lies between an energy range of roughly 20–30 eV below and 40–50 eV above the main absorption edge. XANES data can provide information about the bonding with the neighboring atoms, electronic structure of the interested atom in the materials and support the determination of local atomic arrangements in the materials. However, the EXAFS region is located approximately 40–80 eV above the absorption edges and it is a result of the interference of the wave functions of the outgoing photoelectrons with the backscattered photoelectrons from the neighboring atoms. The EXAFS data can provide rich information about the environment of the source atoms and attracts great interest of the scientists dealing with the crystal structure analysis. From the collected EXAFS data, photoelectron scattering information "chi" (χ) can be estimated according to the formula;

$$\chi = \frac{[\mu(E) - \mu_o(E)]}{\Delta\mu_o} \quad (1)$$

where μ denotes the absorbing coefficient. Besides, the chi signal can also estimated via the formula containing the parameters for the scattering of the photoelectrons and known as the EXAFS equation;

$$\chi(k) = \frac{\Sigma[(N_j f_j(k)\exp(-2k^2\sigma_j{}^2))}{(kR_j{}^2)]\sin[2kR_j + \delta_j(k)]} \quad (2)$$

where "$\delta_j(k)$" is the scattering phase shift, "$f(k)$" is the scattering amplitude, "N" is the coordination number of the neighboring atom, "R" is the distance of the neighboring atom and "$\sigma_j{}^2$ " is the mean-square disorder with the neighboring atom distances.

In this manner, it is possible to extract the information about the local geometrical structures, i.e. bond lengths, coordination numbers and the angles between atoms from experimental EXAFS spectra [6]. Additionally, the periodicity of the oscillations in the region allows us to decide the bond lengths, the amplitudes of the

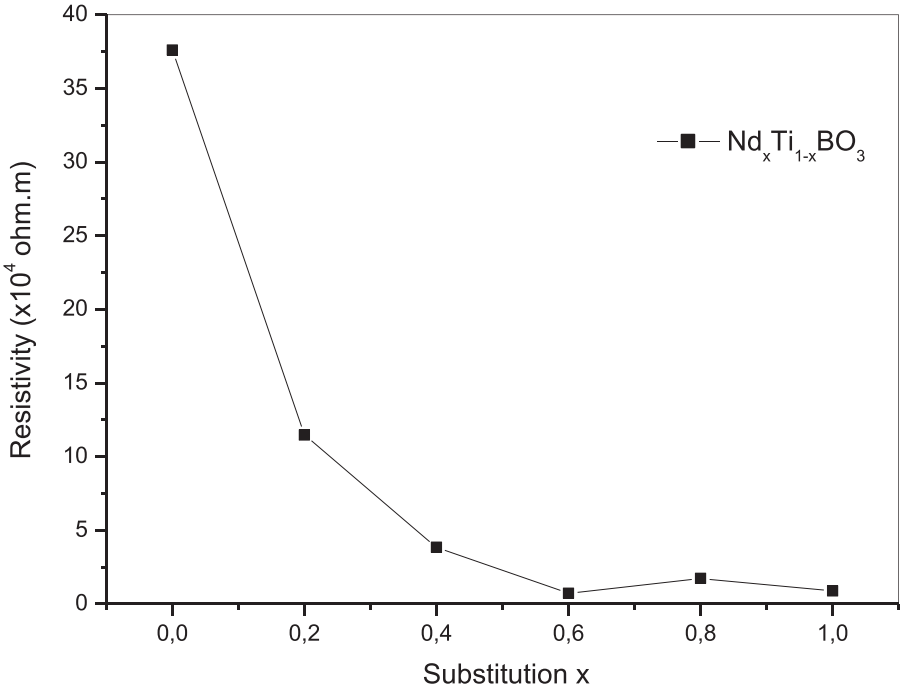

Fig. 1. The electrical resistivity results of Nd-doped $TiBO_3$ samples.

fine structure and provides information about the number of atoms that surround the absorbing atom [6,7].

XAFS data were collected at Beamline-BL8 of Siam Photon (SLRI) Synchrotron Radiation facility in Nakhon Ratschasima, Thailand [8,9]. The beamline operates for X-ray absorption spectroscopy (XANES and XANES) and serves a high flux light from a bending magnet and has an energy range of 1.25–10 keV. The measurements were performed at room temperature in transmission mode for Nd L_3-edge and Ti K-edge. The data for the EXAFS analysis were derived from the measured XAFS spectra by ATHENA and ARTEMIS softwares [9]. The ATHENA software can extract the EXAFS data from the XAFS spectra. Accordingly, for further analysis on the crystal structure would carried out by ARTEMIS software with the generated paths from the FEFF calculations to make fits.

To unveil the exact electronic and crystallographic information from the collected data, the XAFS measurements were supported by calculations. Nd L_3-edge and Ti K-edge XAFS calculations of $Nd_xTi_{1-x}BO_{2+d}$ performed by FEFF 8.2 code, which is based on real space multiple scattering approach [7]. For the calculations the FEFF input files generated by the ATOMS package [10]. The input file of the full multiple scattering calculation for 1.2 nanometer thick rutile TiO_2 cluster, containing 697 atoms (Ti, O) and a Ti atom has selected as the absorber, also a photoelectron emitter. For the samples $Nd_xTi_{1-x}BO_{2+d}$, the input files were generated for Nd L-edge with the same parameters. During the calculations, backscattering and phase shifts with single and multiple scattering paths were also calculated.

3. Results and discussion

To determine the electrical properties of the samples, the electrical resistivity measurements were performed at the MEITAM labs. of Mersin University with four-probe technique. The results of the measurements for $Nd_xTi_{1-x}BO_{2+d}$ samples are given in Fig. 1. Unlike with the reported study of Xu et al., the $TiBO_3$ sample showed higher electrical resistivity than Nd substituted samples, but not "an insulator" and all the substituted samples fall in the category of semiconductors. The resistivity of the $TiBO_3$ sample highlighted a different crystal structure formation other than the reported one in the paper of Xu et al.. Also, the response of the electrical resistivity to the Nd substitution process reveals with a sharp decrease and give better semiconductor results. In the other words, Nd substitution causes a disturbance in the $TiBO_3$ which provides better electrical conductivity properties at room temperatures. Especially, for $x = 0.6$ and 1, the samples have lower and close resistivity values pointing out a joint structure formed in both samples.

To identify the background information of the electrical properties, we need to understand the structure properties in the samples that can provide us useful data for further crystal structure analysis. Therefore, XRD patterns of the samples were taken with Rigaku Smartlab model. In Fig. 2, XRD patterns of the samples are given in comparison with $TiBO_3$ and the substituted samples. Crystal structure analysis were performed by the MAUD software on the collected XRD patterns [11].

The smooth pattern of the sample for $x = 0$ (i.e. $TiBO_3$) highlights a more uniform crystal structure among others with lower noise, like $NdBO_3$. The $TiBO_3$ crystal were reported to form in Rhombohedral structure with "R-3 c" space group symmetry [4]. However, in this study, the $TiBO_3$ sample was determined in tetragonal $TiB_{0.024}O_2$ structure as reported elsewhere [12]. The determined crystal structures for the samples are given in Table 1. The reason for the notable Boron and Oxygen deficiency leading to $TiB_{0.024}O_2$ structure rather than $TiBO_3$ is the main question in the study. The boron atoms were determined to bond with oxygens strongly due to higher electronegativity than titanium atoms and formed oxide complexes who prevent Boron to bond directly by forming $TiBO_3$ layers. As the crystal structure defined in sample $x = 0$ pointed out that only a small amount of Boron remained in the samples bonding with Ti atoms. As a result, Ti-B bonds only formed as the rutile $TiB_{0.024}O_2$ layers. It is due to the melting of the isolated Boron–Oxide complexes during the annealing process over 500 °C.

With the 20% Nd substitution, i.e. $x = 0.2$, the pattern became noisy and highlights a crystal structure formation with a lower symmetry than the rutile. According to the crystal analysis, the sample with $x = 0.2$ were formed in monoclinic $NdTi_3B_2O_6$ structure with a space group of "P21/c:b1". Yet now, the crystal structure for Nd–Ti complexes has not been reported in the literature. The small amount of the substituted Nd atoms and their

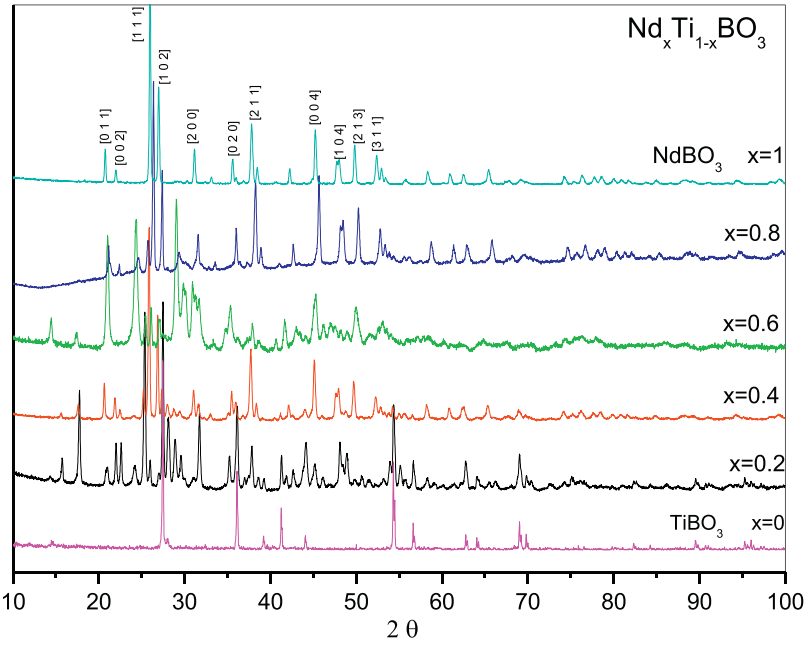

Fig. 2. Comparison of XRD patterns of $Nd_xTi_{1-x}BO_3$ samples.

Table 1
The XRD pattern results of Nd substitution in $TiBO_3$ samples.

Substitution ($Nd_xTi_{1-x}BO_3$)	Crystal	α	β	γ	a	b	c	Geometry	SG	%
$X=0$	$TiBO_2$	90	90	90	4.593	4.593	2.959	Tetragonal	P42/mnm	100
$X=0.2^*$	$NdTi_3B_2O_6$	90	121.50	90	6.654	8.879	12.075	Monoclinic	P21/c:b1	100
$X=0.4^*$	$TiBO_2$	90	90	90	4.493	4.493	2.947	Tetragonal	P42/mnm	56
	$Nd_2Ti_3B_4O_{12}$	90	90	90	8.896	15.814	7.336	Orthorhombic	Pc221n:bca	44
$X=0.6$	$Nd_2Ti_3B_4O_{12}$	90	90	90	8.382	17.683	7.429	Orthorhombic	Pc221n:bca	61
	$NdBO_3$	90	90	90	6.326	6.516	6.540	Triclinic	P-1	39
$X=0.8^*$	$NdTiB_5O_{10}$	90	93.18	90	8.629	7.723	9.476	Monoclinic	P21/c:b2	70
	$NdTiBO_5$	90	96.91	90	9.872	7.387	5.361	Monoclinic	P21/c:b1	30
$X=1.0$	$NdBO_3$	90	90	90	5.740	5.040	8.080	Orthorhombic	Pnma	100

relations with the environment were determined as the source of the new structure and lower symmetry.

The noisy and multipeak XRD pattern of the sample have about the same characteristics in $x=0.4$ and $x=0.6$. But, the decrease in the noisy structure provide us an image of the crystal transformation to a new structure with richer symmetry governed by the increasing Neodymium (Nd) atoms. Starting from the sample for $x=0.4$, some Nd sites formed in orthorhombic crystal geometry as $Nd_2Ti_3B_4O_{12}$ with "Pc221n:bca" space group symmetry with a percentage of 44% in entire bulk, which is also new to literature. It is interesting that, rest of the atoms in the crystal formed in $TiB_{0.024}O_2$ structure (56%). Higher Boron concentration in the $Nd_2Ti_3B_4O_{12}$ structure may forced up the rest of the Borons to form in $TiB_{0.024}O_2$.

In the sample with $x=0.6$ substitution, with the increasing number of Ti atoms in the samples, no rutile $TiB_{0.024}O_2$ structure were observed, but mainly $Nd_2Ti_3B_4O_{12}$ structure was remained in the crystal with a percentage of 61%. Due to the decrease in Ti amounts in the bulk, $NdBO_3$ structure formation with Triclinic geometry and "P-1" space group was determined. This improves that the change in the ratios of the Ti and Nd atoms force them to build up crystal structures of higher symmetries both for Nd and Ti and the rest tend to form in a most possible formation with their lesser amounts. Like in the samples with $x=0.4$ and 0.6 substitution, they have a dominant structure; Orthorhombic $Nd_2Ti_3B_4O_{12}$ where they both have similar amounts.

The decrease in the noisy structure with higher peak intensities in the XRD pattern of the sample with $x=0.8$, highlights the phase transformation to a more uniform crystal structure. The sample was determined to have a polycrystal structure and formed in two different phases but in the same geometry. In the sample, two new crystal structure formation for Nd–Ti complexes were determined as: (70%) $NdTiB_5O_{12}$ structure with monoclinic geometry having "P21/c:b2" space group symmetry and (30%) $NdTiBO_5$ structure with monoclinic geometry having a space group symmetry of "P21/c:b1". The lower crystal symmetries of the structures are compatible with the increase in the electrical resistivity at $x=0.8$.

The sample for $x=1$ was determined to have only Orthorhombic $NdBO_3$ structure with "Pnma" space group. The single crystal structure and its rich symmetry result a fine XRD pattern and lowest electrical resistivity among other samples.

To identify the reasons for different crystal formations in the samples, the electronic structure study with XANES spectroscopy is a good choice that can provide useful informations. For the 3d transition metals, K-edges are so sensitive to the interactions with the neighboring atoms and the chemical states of the atoms, where

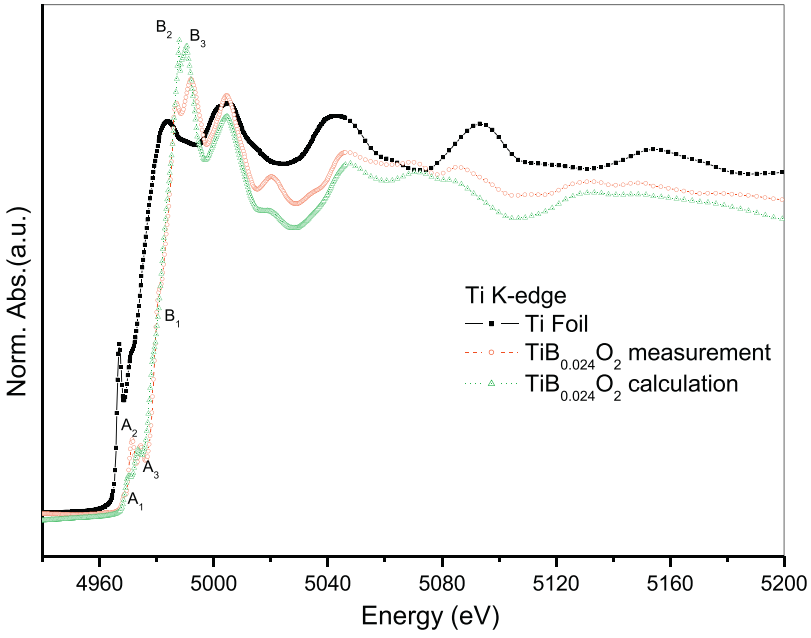

Fig. 3. Compared XAFS spectra of Ti K-edges of the metal Ti with measured and calculated $TiB_{0.024}O_2$ spectra.

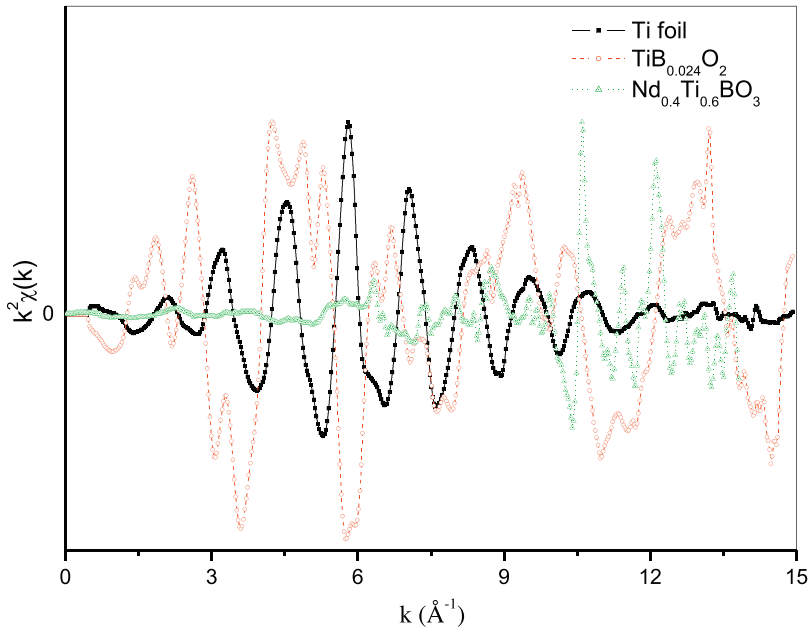

Fig. 4. The comparison of the EXAFS chi data for Ti foil, $TiB_{0.024}O_2$ and $Nd_{0.4}Ti_{0.6}BO_3$.

1s electrons transition to the empty levels over the Fermi level as a final state takes place. For 1s electrons transition to 3d level as a final state are forbidden according to quantum selection rule. The 3d level are located below the Fermi level and can give clues about the bonding properties of the source atoms.

The XANES region can be studied into three regimes; the pre-edge, main-edge and the post-edge. The pre-edge structure lies just below the main absorption edge and highlights the forbidden transitions, crystal disorders, asymmetries etc., i.e., gives a picture of disorders in the structure. At the same time, the post-edge part lies just beyond the main edge and provides information about the interactions with the closest neighboring atoms.

In the study, the rutile $TiB_{0.024}O_2$ and orthorhombic $NdBO_3$ samples were selected as the reference materials to observe and compare the changes both in the crystal and electronic structures. The measured Ti K-edge spectra of the Ti foil is given with the measured and calculated spectra of the $TiB_{0.024}O_2$ sample in Fig. 3. For the calculations, the input data were created according to the determined lattice parameters for the rutile $TiB_{0.024}O_2$ structure from the XRD analysis. In the figure, the measured $TiB_{0.024}O_2$ spectra have a high agreement with the calculated spectra. However, the pre-edge and main edge structures have slight differences, making the weak boron contributions visible. Also, $TiB_{0.024}O_2$ sample has an energy shift to higher photon energy values about ~6 eV. The shift is related to the oxidation state of Ti atoms in the $TiB_{0.024}O_2$ and emphasizing electron gain during molecular interactions. The pre-edge structure of the Ti K-edge are attributed to the 1s electrons forbidden transition to the 3d empty states. The measured XANES spectra of the K-edge shows that the pre-edge structure exists in the nature of Titanium (p–d mixing)

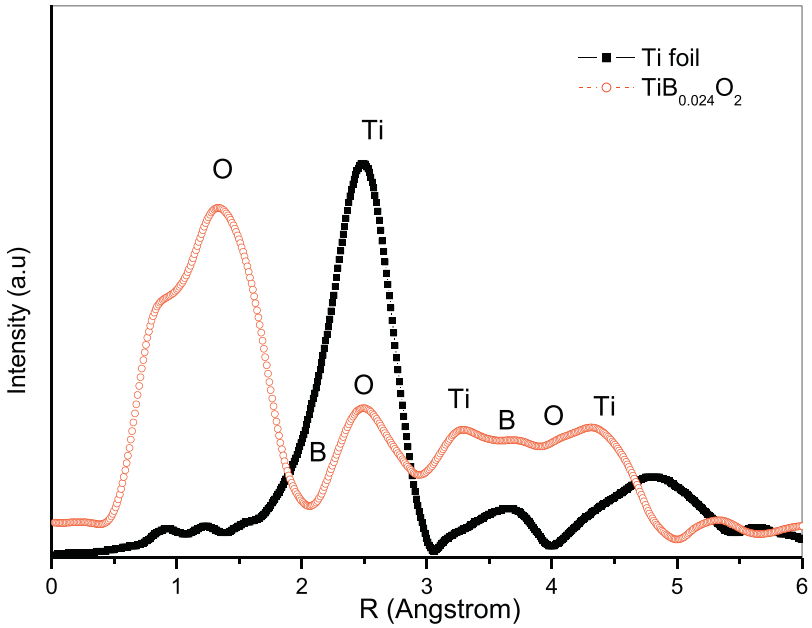

Fig. 5. Compared radial distribution function (RDF) results of the Ti foil and $TiB_{0.024}O_2$.

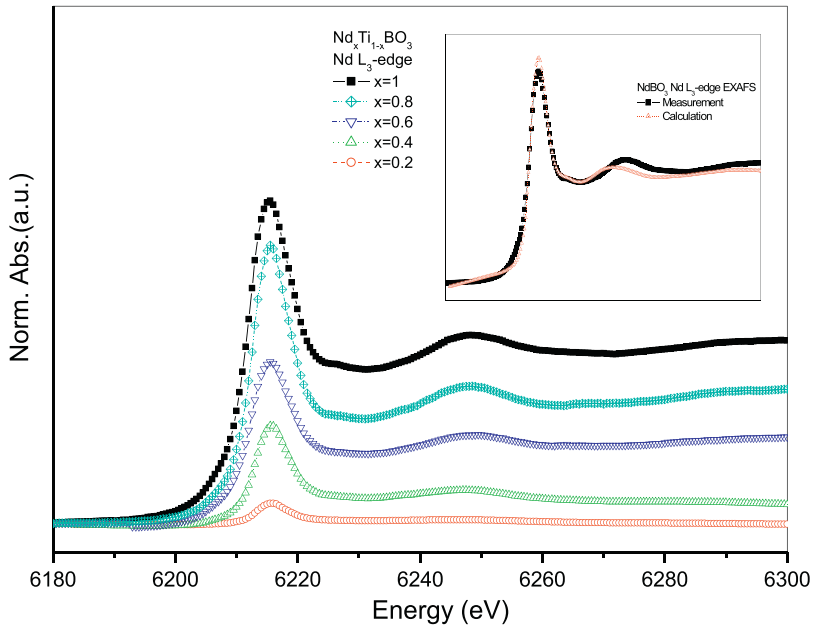

Fig. 6. Comparison of the Nd L_3-edge XANES spectra of the Nd doped samples.
Inset: comparison of the measured and calculated Nd L_3-edge XANES spectra in $NdBO_3$.

and its compounds. Obviously, the $TiB_{0.024}O_2$ spectra have larger pre-edge structure with more peaks that means a stronger hybridization between Ti and O with a weak B contribution. The measurement has a more intense pre-edge and a two-peak main edge, which is different from the calculation where only a small amount of Boron were considered.

In the figure, the spectra begins to rise at 4965 eV. The pre-edge peaks, labeled as A_1, A_2, A_3 are due to the quadrupolar transitions from 1s to 3d low energy levels t_{2g} with the support of rich p symmetries by O and B 2p level hybridizations. The absorption peak energies of the pre-edge peaks are 4968.9 eV, 4971.5 eV and 4974.2 eV, respectively. The B_1 peak is assigned to the hybrid low energy levels of O 2p with Ti 4p levels, where B_2 and B_3 levels are due to 1s–4p transitions of electrons with strong spin-orbit coupling. Additionally, the absorption peak energies of the B_1, B_2 and B_3 peaks are 4980.4 eV, 4987.1 eV and 4990.2 eV, respectively.

In Fig. 4, the extracted chi (χ) signals of metal Ti, $TiB_{0.024}O_2$ and $Nd_{0.4}Ti_{0.6}BO_{2+d}$ samples are given in comparison. In the comparison, $Nd_{0.4}Ti_{0.6}BO_{2+d}$ sample were chosen as an example to show the structural differences of the substituted samples. With its single crystal structure and one atom type content, metal Ti sample has more smooth chi signals. However, the noisy structure of the $TiB_{0.024}O_2$ highlights the lower symmetry of the geometry and non-homogeneous crystal geometry in the entire bulk. The chi signals of the $Nd_{0.4}Ti_{0.6}BO_{2+d}$ sample have the most noisy structure with the lowest intensities at higher k values. This highlights shorter path lengths of photoelectrons due to rapid energy loss

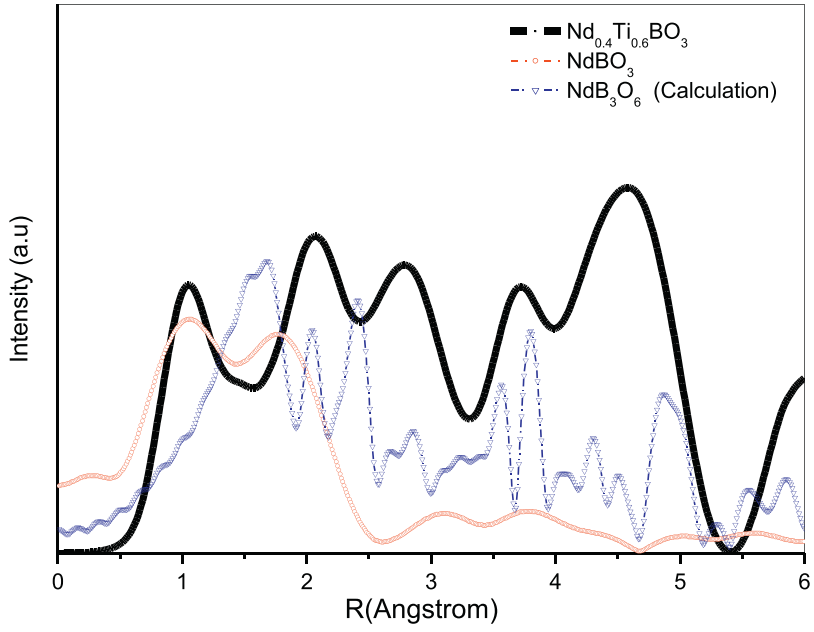

Fig. 7. Compared radial distribution function (RDF) results of the $NdBO_3$, $Nd_{0.4}Ti_{0.6}BO_3$ and calculated NdB_3O_6 structure.

Table 2
Radial distribution function (RDF) analysis results for the closest neighbors of Nd in the sample $Nd_{0.4}Ti_{0.6}BO_3$.

Compound	Source atom	Type of atom	Distance (Å)	Debye–Waller factor; σ^2(Å^2)	Degeneracy
$Nd_{0.4}Ti_{0.6}BO_3$	Nd	O	2.38	0.0139	1
		B	2.95	0.0224	1
		Ti	3.92	0.0060	2
		Nd	3.99	0.0029	2

because of frequent scattering from different types of atom in a more dense crystal. Besides, the signals have narrower bandwidths than Ti metal because of shorter distances. To clarify the disturbance in the atomic levels in the structure, the Fourier transform of the EXAFS chi signals, the radial distribution function (RDF) data can provide us a better tool to analyze. RDF relates to the one dimensional localization of the neighboring atoms surrounding the source atom.

In Fig. 5, the RDF result of the $TiB_{0.024}O_2$ sample are given in comparison with the Ti foil. For $TiB_{0.024}O_2$ structure, light atoms (O and B) are located between heavier Ti atoms and the distance to the closest Ti atoms, where a Ti atom sits at the origin. Distance between two neighboring Ti atoms were estimated with a distance of 3.67 Å (angstroms). However, in the metal Ti sample, the closest distance for neighboring Ti atoms was estimated as 2.95 Å. The multipeak structures in the $TiB_{0.024}O_2$ sample are due to the signals from the light atoms (O, B) located between two neighboring Ti locations. Light atoms bond with Ti atoms and force them to relocate far with each other with the effect of B complexes. Besides, wider peaks is a result of different symmetry in a location which means the same atoms may locate with slightly different angles yield overlapped signals.

As discussed above with the XRD patterns, the Nd substitutions were observed to cause disturbance in the $TiBO_3$ structure for small x values (0.2 and 0.4) leading to new structure formations. However, beyond the half concentration of the substitution process (i.e., 0.6), the substituted Nd atoms became dominant and built an orthorhombic structure, which has a more stable composition. To reveal the mechanisms leading to the desired properties for these materials, XAFS analysis of Nd atoms can provide rich data for the study. It is a good choice to obtain better results that can provide us both electronic and crystal structure picture with a wide view from the Nd side.

In Fig. 6, the Nd L_3-edge XANES spectra are given in comparison with all "x" values for this study. In the inset of the figure, the measured spectra of the orthorhombic $NdBO_3$ sample is given with its FEFF 8.2 calculation, which exhibits a good agreement. Nd L_3-edge absorption spectra have a meaningful decay in the intensity which is parallel to the Nd concentration in the bulk. The L_3-edge of Nd is due to the excited 2p electrons transition to unoccupied 5d levels as a final state. The spectra begin to rise from the photon energy of 6192 eV and have a maximum at 6215.25 eV. According to the collected data, no shifts in the symmetry of the maxima were observed. The symmetry means that the Nd atoms almost have the same environment on the structure in all doped samples. 4f level of the Nd metal has possible vacancies for the 2p electrons, however transition from 2p to directly 4f level is forbidden according to the quantum selection rules (i.e. $\Delta l = \pm 1$). The Nd L_3-edge spectrum has no significant pre-edge structure which means no forbidden transition occurs. However, wide absorption slope below main edge maximum gives us a clue about the existence of 4f–5d mixed large molecular band. Besides, on the absorption spectra of the sample for $x = 1$, there exist a vague raise at about 6205 eV confirming the mixing at the valence levels. The main route for 2p electrons are 2pà5d transition, but neighboring O atom valency level give support to the 4f electrons to be actively involved in the interactions via $2p^5 4f^4 5d^1$ hybridization and build a large band with rich quantum symmetry as a final state.

In Fig. 7, the RDF data on the $Nd_{0.4}Ti_{0.6}BO_{2+d}$ structure are given. As a guide to compare the atomic locations of the $Nd_{0.4}Ti_{0.6}BO_{2+d}$ sample, measured RDF data of the $NdBO_3$ are presented with the RDF calculations of NdB_3O_6 (as a reference for most common structure) and rutile $TiB_{0.024}O_2$ in the same figure. The multipeak structure of the $Nd_{0.4}Ti_{0.6}BO_{2+d}$ sample presents a clear image of the complicated crystal formation inside the material. It is a result of the unstable polycrystalline structures as determined by the XRD analysis. Besides, due to presence of oxygen in different Ti or Nd based geometries, the Oxygen atoms possess locations with slight different distances and angles resulting overlapped signals. As a result of the RDF study, the atomic distances for the nearest O, B, Ti and Nd atoms to the source Nd atoms are given with the estimated Debye Waller factors in Table 2.

4. Conclusion

In this study, crystal structure and electronic properties of $Nd_xTi_{1-x}BO_{2+d}$ structure were investigated by XAFS measurements. The crystal structure disturbances were determined as a result of the increasing Nd substitutions by both XRD patterns and XAFS analysis. In the early stages of the substitutions, distortions in the Ti geometries were observed due to the increasing substitution amounts of Neodymium in the samples and the deficiency in Boron concentrations. For 0.2, 0.4 and 0.8 values of "x", Nd atoms were determined to form new crystal structures where formed Nd–Ti complexes were observed. Besides, for the sample $x = 1$, Nd atoms were determined to form in a stable orthorhombic structure and it was determined to have a better electrical conductivity.

Acknowledgements

The author would like to thank to Dr. Wantana Klyusubun and the staff of BL8 from SLRI (Siam Photon) of Thailand, both for their technical support and great hospitality.

This study was supported financially by "BAP-TTEF EEEME (OMÖ) 2012-7" project of Mersin University (Mersin, Turkiye).

References

[1] C. Ruihua, C.N. Borca, P.A. Dowbena, S. Stadler, Y.U. Idzerda, Appl. Phys. Lett. 78 (4) (2001) 521.
[2] H.S. Nabi, R. Pentcheva, Phys. Rev. B 83 (2011) 214424.
[3] A. Moore Elaine, Phys. Rev. B 76 (2007) 195107.
[4] Y.W. Liu, X.F. Rui, Y.Y. Fu, Y.W. Han Zhang, J. Metastable Nanocryst. Mater. 23 (2005) 243.
[5] Z. Xu, M.K. Matam, Z.G. Ye, American Physical Society, Annual March Meeting 2001 March 12–16, Washington State Convention Center Seattle, Washington Meeting ID: MAR01, 2001 abstract #K40.077.
[6] A.L. Ankudinov, B. Ravel, J.J. Rehr, S.D. Conradson, Phys. Rev. B 56 (1997) R1712.
[7] B. Ravel, J. Synchrotron Radiat. 8 (2) (2001) 314.
[8] W. Klysubun, et al., Commission and performance of X-ray absorption beamline at the Siam Photon Laboratory, Nucl. Instrum. Methods Phys. Res. (2007) A582:87W.
[9] Klysubun, et al., AIP Conference Proceedings, X-ray absorption spectroscopy beamline at the Siam Photon Laboratory, 8792006, pp. 860.
[10] B. Ravel, M. Newville, J. Synchrotron Radiat. 12 (4) (2005) 537.
[11] L. Lutterotti, M. Bortolotti, IUCr: Comput. Newsletter 1 (2003) 43.
[12] I.E. Grey, C. Li, C.M. MacRae, L.A. Bursill 127 (240) (1996) .